Supporting Information

Foijer et al. 10.1073/pnas.1400892111

SI Materials and Methods

Generation of Mps1^{f} Conditional and Mps1$^{\Delta}$ Mutant Mice. A 129/Sv mouse genomic λ-phage library was screened for the genomic locus of monopolar spindle 1 (*Mps1*) as described (1). A 14-kb portion of the *Mps1* genomic locus encoding exons 1–9 was isolated and cloned into pBluescript (Life Technologies) via NotI sites. DNA encoding diphtheria toxin A was cloned into the NotI site as a negative selection marker. A loxP site was cloned into an NcoI site between exons 2 and 3. A 4-kb selection cassette containing thymidine-kinase and the neomycin-resistance gene flanked by two loxP and FRT recombination sites (LFNT cassette) was cloned into a SphI site between exons 4 and 5. The resulting 22.6-kb targeting vector (Fig. S1*A*, line 2) was introduced into ES cells, and clones were isolated as previously described (1). Incorporation of the gene-targeting vector by homologous recombination into ES clones was determined by Southern blotting as described (1), using a 664-bp 5′ probe and a 665-bp 3′ probe after digestion with NheI or BglI as indicated in Fig. S1*A*, line 3. The 5′ probe was generated by digesting a λ-phage clone with SacI and XmaI which contained sequences 5′ of the targeting vector and then was subcloned into pBluescript (Life Technologies). The 5′ probe yields an 11.7-kb wild-type band and a 9-kb targeted band. The 3′ probe is homologous to sequences containing exon 9 of Mps1 and was generated by PCR yielding a 13.4-kb wild-type band and a 9.4-kb targeted band. Two correctly targeted ES clones were isolated. The LFNT cassette was removed in these ES clones by transfecting cells with vectors expressing Cre recombinase (pCrePac) or flippase recombinase (pFlpe), resulting in the kinetochore-binding domain deletion (DK) (Fig. S1*A*, line 5) or conditional (f) (Fig. S1*A*, line 4) allele, respectively. Southern blotting after restriction/digestion with NcoI and probing with the 5′ 664-bp probe yielded 8 kb for wild type, 12 kb for the targeted locus (containing LFNT), 15.2 kb for the DK allele, and 18.6 kb for the f-allele. Three DK^{+} and two f^{+} subclones from the two original clones were injected into blastocysts and successfully generated founder lines for the conventional DK and conditional alleles.

To assess the consequences of Mps1 truncation in developing embryos, we generated *Mps1*$^{\Delta/+}$ ES cells by Cre electroporation, established the *Mps1*^{DK} allele in the germ line, and intercrossed *Mps1*$^{DK/+}$ mice. No *Mps1*$^{DK/DK}$ mice were recovered in 33 litters comprising 237 pups, showing that the Mps1 truncation allele is embryonic lethal (*Mps1*$^{+/+}$ mice comprised 38% of viable pups, and *Mps1*$^{DK/+}$ mice comprised 62% of pups, the expected Mendelian ratio) (Fig. S5*B*). At embryonic day 10.5 (E10.5), embryos were isolated, and the yolk sac was taken to determine genotype by PCR as described (2). *Mps1*$^{DK/DK}$ embryos died at or before E10 (Fig. 5*C*), as previously described with the germ-line deletion of other checkpoint genes (3–5). We conclude that aneuploidy generated by the *Mps1*^{DK} allele is lethal to developing embryos.

Generation of pRetrox GFP-Mps1 Full-Length, pRetrox GFP-Mps1DK, and Cre-T2A-GFP. For pRetrox GFP-Mps1 vectors, we first PCR amplified EGFP (Phusion polymerase; Thermo Scientific) with BglII and BamHI+NotI Sites 5′ and 3′ respectively. This PCR fragment was cloned into BamH1-, and NotI- (New England Biolabs) digested pRetrox backbone (Clontech), thus destroying the BamH1 site 5′ of the GFP. In the case of full-length Mps1, we then PCR-amplified Mps1 from a human *Mps1* cDNA clone (DNA Resource Core, Dana-Farber/Harvard Cancer Center) flanked by BamH1 and NotI sites 5′ and 3′ respectively, which was cloned into pRetrox-eGFP digested with BamH1 and NotI. For Mps1^{DK}, we first PCR-amplified a fragment encompassing the 5′ ATG to an endogenous HindII site in exon 1 of human *Mps1*, which was ligated into a pMSCV backbone (Clontech), harboring the mouse stem cell virus (MSCV) LTRs, digested with BamH1 and HindIII. We next PCR-amplified Mps1 from the start of exon 4 to its stop codon and added the remaining exon 1 sequence downstream of the HindIII site to the 5′ end of this product, resulting in a HindIII–NotI fragment. This fragment was ligated into the product of the previous step, thus creating Mps1^{DK}. We then PCR-amplified Mps1^{DK} from pMSCV Mps1^{DK} using BglII and NotI sites and cloned it into pRetrox eGFP as we did for full-length Mps1. For Cre-T2A-GFP, we first PCR amplified GFP, adding a T2A sequence flanked by BglII and BamH1-NotI sites to its 3′ end (6), and cloned it into pRetrox using BamH1 and NotI sites. We next cloned Cre downstream of GFP-T2A using BamH1 and NotI sites 5′ and 3′, respectively. All primers used are listed in Dataset S5.

Quantification of Kinetochore-Bound Mps1. To quantify the levels of GFP-Mps1 bound to kinetochores, fluorescence arbitrary units on a horizontal line through a kinetochore were analyzed in SoftWorx software (GE Healthcare) using the line-profiling tool. To correct for GFP-tagged protein expression levels, we normalized kinetochore-bound values by subtracting the average GFP expression counts in the cell from the counts at the kinetochore (line-profiling tool). We then calculated the fluorescence ratios between GFP-Mps1 and GFP-Mps1^{DK} for both cell types (Fig. S1 *E* and *G*).

Comparative Genome Hybridization and Analysis. For array-based comparative genomic hybridization (aCGH) experiments DNA was labeled with Cy3 or Cy5 fluorescent nucleotides according to the BioPrime array CGH genomic labeling protocol (Life Technologies) and cleaned using the PureLink PCR purification kit (Life Technologies). Many liver samples showed evidence of T-cell infiltration, disqualifying them as control samples. Therefore we used pooled sex-matched reference samples from uninfiltrated livers from littermates. Labeled DNA was hybridized to 244K mouse genome CGH microarrays (Agilent) according to the manufacturer's protocol and subsequently was scanned, background corrected, and normalized using the loess algorithm with Bioconductor limma package (7). Data then were segmented and split into regions of estimated equal copy number using a circular binary segmentation algorithm (Bioconductor) with the DNAcopy package (8). To reduce noise further, we used the "undo" method to remove all splits that are not at least 3 SDs apart. Log2 ratios of tumor to/reference were plotted along the chromosome coordinates using the same software. To create a multisample matrix, we assigned segment means to mouse genes [National Center for Biotechnology Information (NCBI) M37 and M63] on all segments for each sample using the Bioconductor CNTools package. Data were processed further and sorted by chromosomal position in Microsoft Excel. The aneuploidy score was calculated by assessing whole-chromosome losses and gains in Agilent Genomic Workbench software, and statistical analyses were performed using GraphPad Prism software. To find chromosome regions showing common gains/losses, we computed segment gain or loss (SGOL) scores by calculating all positive and negative log2 ratio values over or under a log2 ratio threshold (|0.3|) using the Bioconductor cghMCR package (9).

RT-PCR, Quantitataive PCR, and Expression Arrays. Synthesis of biotin-labeled cRNA was performed using an Illumina TotalPrep RNA amplification kit (Ambion). Amplified biotinylated cRNA (1.5 μg) was hybridized to llumina Sentrix BeadChips (v6.2) and subsequently labeled with streptavidin-conjugated Cy3 (Amersham) according to the manufacturer's protocol. After scanning, data were quantile normalized (10) and analyzed using the Bioconductor lumi (11) and limma packages (7). Data were adjusted by *P* value to yield a sorted list of differentially expression genes (12) and were sorted by chromosomal position or frequency of deregulation in Microsoft Excel. For Gene Ontogeny analysis, all genes with log2 values between −0.6 and 0.6 (less than 1.5-fold deregulated) and genes deregulated in fewer than four tumors were excluded. For RT-PCR, reverse transcription was performed using an OligoDT, random hexamer mixture and Molony murine leukemia virus-RT (New England Biolabs) according to the manufacturer's instructions. Primer sequences can be found in Dataset S5. For quantitative PCR (qPCR) reactions, 1 μg of total RNA was used for a reverse transcriptase reaction (Superscript II; Life Technologies). The resulting cDNA was used as a template for qPCR (ABI PRISM 7700 Sequence Detector) in the presence of SYBR-Green (Life Technologies) to label the product. The relative amounts of cDNA were compared with actin to correct for the amount of total cDNA. Average values and SDs were calculated as indicated in figure legends and were compared with the expression values in control mice (normalized to the value of 1). Primer sequences are listed in Dataset S5.

1. Dobles M, Liberal V, Scott ML, Benezra R, Sorger PK (2000) Chromosome missegregation and apoptosis in mice lacking the mitotic checkpoint protein Mad2. *Cell* 101(6):635–645.
2. Burds AA, Lutum AS, Sorger PK (2005) Generating chromosome instability through the simultaneous deletion of Mad2 and p53. *Proc Natl Acad Sci USA* 102(32): 11296–11301.
3. Foijer F, Draviam VM, Sorger PK (2008) Studying chromosome instability in the mouse. *Biochim Biophys Acta* 1786(1):73–82.
4. Schvartzman JM, Sotillo R, Benezra R (2010) Mitotic chromosomal instability and cancer: Mouse modelling of the human disease. *Nat Rev Cancer* 10(2):102–115.
5. Holland AJ, Cleveland DW (2009) Boveri revisited: Chromosomal instability, aneuploidy and tumorigenesis. *Nat Rev Mol Cell Biol* 10(7):478–487.
6. Szymczak AL, et al. (2004) Correction of multi-gene deficiency in vivo using a single 'self-cleaving' 2A peptide-based retroviral vector. *Nat Biotechnol* 22(5):589–594.
7. Smyth GK (2005) *Limma: Linear Models for Microarray Data* (Springer, New York), pp 397–420.
8. Venkatraman ES, Olshen AB (2007) A faster circular binary segmentation algorithm for the analysis of array CGH data. *Bioinformatics* 23(6):657–663.
9. Aguirre AJ, et al. (2004) High-resolution characterization of the pancreatic adenocarcinoma genome. *Proc Natl Acad Sci USA* 101(24):9067–9072.
10. Yang YH, et al. (2002) Normalization for cDNA microarray data: A robust composite method addressing single and multiple slide systematic variation. *Nucleic Acids Res* 30(4):e15.
11. Du P, Kibbe WA, Lin SM (2008) lumi: A pipeline for processing Illumina microarray. *Bioinformatics* 24(13):1547–1548.
12. Benjamini Y, Hochberg Y (1995) Controlling the false discovery rate: A practical and powerful approach to multiple testing. *J R Stat Soc, B* 57(1):289–300.

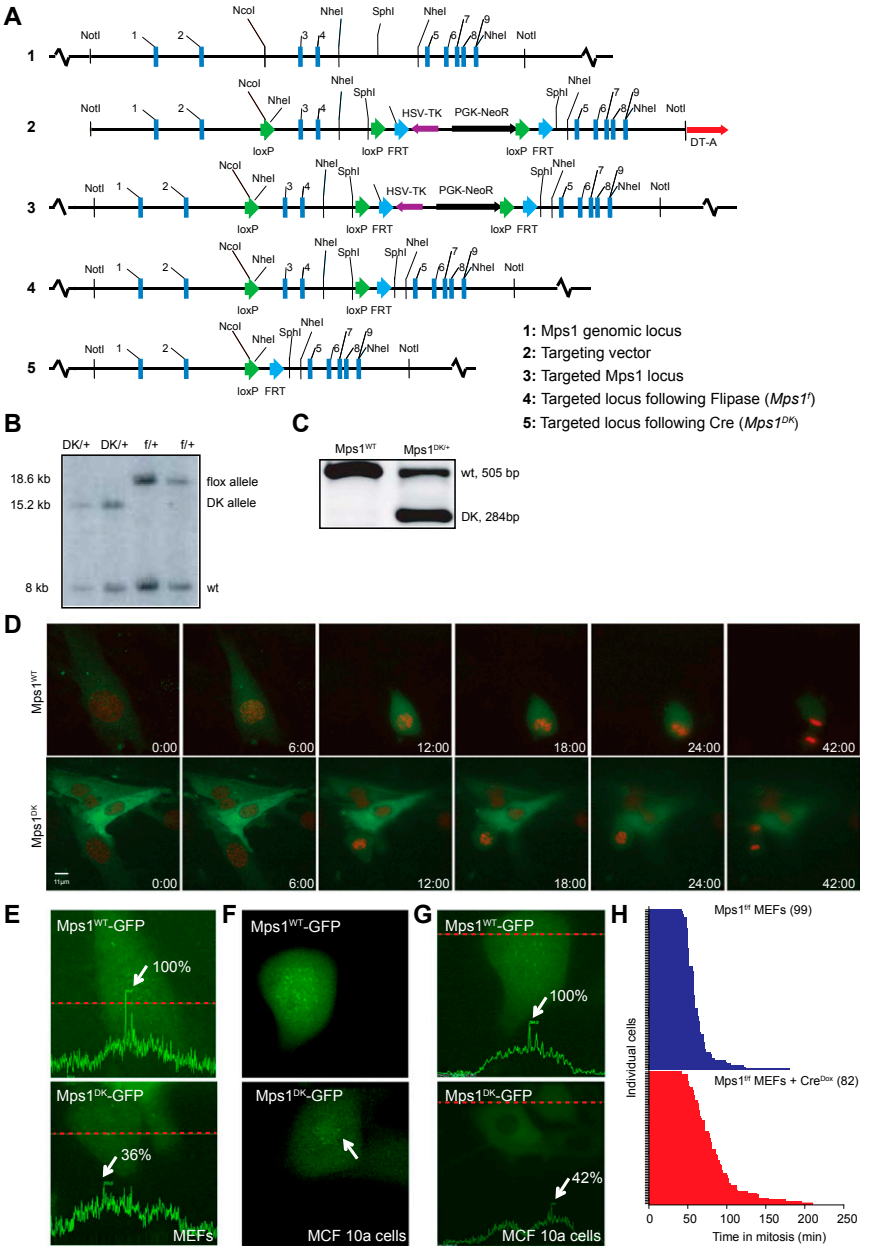

Fig. S1. Engineering a conditional *Mps1* allele showing severely decreased kinetochore binding in mitosis. (*A*) Schematic overview of the *Mps1* locus, the conditional targeting vector, and targeted locus before and after Flp and Cre-recombinase expression. (*B*) Southern blot on tail DNA from founder mice harboring conditional (f) and DK alleles demonstrating germ-line transmission. (*C*) RT-PCR for *Mps1* on mRNA isolated from wild-type and $Mps1^{f/+}$; $Lck\text{-}Cre^{+}$ thymocytes showing expression of the $Mps1^{DK}$ hypomorphic protein. (*D*) Time-lapse image stills showing kinetochore localization of retrovirally transduced wild-type GFP-Mps1 during mitosis (*Upper*) and less binding of GFP-$Mps1^{DK}$ to kinetochores (*Lower*). DNA was labeled with retroviral H2B-Cherry. Also see Movies S1 and S2. (*E*) Quantification on time-lapse image stills (Movies S1 and S2) of kinetochore-bound Mps1 in cells expressing either wild-type GFP-Mps1 (*Upper*) or GFP-$Mps1^{DK}$ (*Lower*) when expressed in mouse embryonic fibroblasts (MEFs). Indicated percentages refer to the average GFP signal on three kinetochores within one cell and compared between cells expressing wild-type GFP-Mps1 and GFP- $Mps1^{DK}$. The dashed red line indicates where the fluorescence signal was quantified. (*F*) Time-lapse image stills showing strong kinetochore localization of retrovirally transduced wild-type GFP-Mps1 in pro-metaphase (*Upper*) and weak kinetochore localization of GFP-$Mps1^{DK}$ (*Lower*) in human MCF 10A cells. DNA was labeled with retroviral H2B-Cherry. See also Movies S3 and S4. (*G*) Quantification on time-lapse image stills (Movies S3 and S4) of kinetochore-bound Mps1 in cells expressing either wild-type GFP-Mps1 (*Upper*) or GFP-$Mps1^{DK}$ (*Lower*) when expressed in MCF 10A cells. The dashed red line indicates where the fluorescence signal was quantified. (*H*) Distribution of mitotic durations for control-infected $Mps1^{f/f}$ (blue) and Cre-infected $Mps1^{f/f}$ (red) MEFs. Average values are shown in Fig. 1*F*.

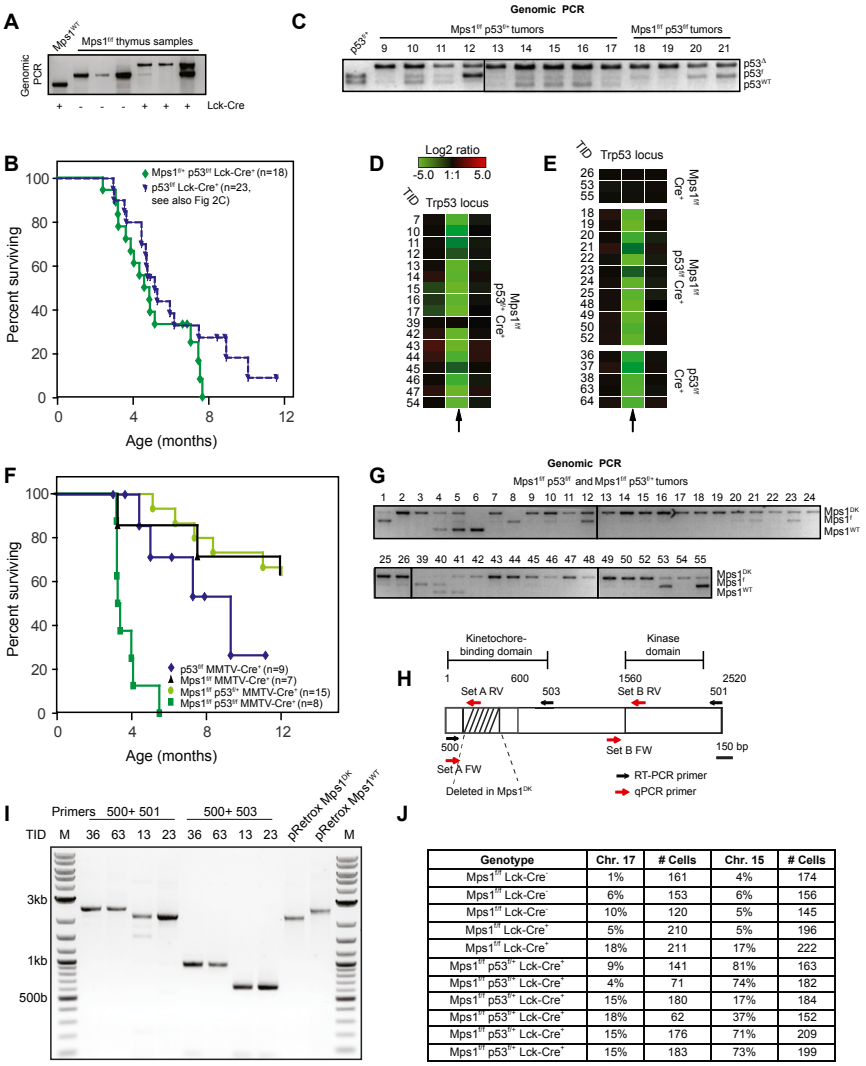

Genotype	Chr. 17	# Cells	Chr. 15	# Cells
Mps1$^{f/f}$ Lck-Cre^{-}	1%	161	4%	174
Mps1$^{f/f}$ Lck-Cre^{-}	6%	153	6%	156
Mps1$^{f/f}$ Lck-Cre^{-}	10%	120	5%	145
Mps1$^{f/f}$ Lck-Cre^{+}	5%	210	5%	196
Mps1$^{f/f}$ Lck-Cre^{+}	18%	211	17%	222
Mps1$^{f/f}$ p53$^{f/+}$ Lck-Cre^{+}	9%	141	81%	163
Mps1$^{f/f}$ p53$^{f/+}$ Lck-Cre^{+}	4%	71	74%	182
Mps1$^{f/f}$ p53$^{f/+}$ Lck-Cre^{+}	15%	180	17%	184
Mps1$^{f/f}$ p53$^{f/+}$ Lck-Cre^{+}	18%	62	37%	152
Mps1$^{f/f}$ p53$^{f/+}$ Lck-Cre^{+}	15%	176	71%	209
Mps1$^{f/f}$ p53$^{f/+}$ Lck-Cre^{+}	15%	183	73%	199

Fig. S2. Mps1 truncation accelerates lymphomagenesis in a p53-deficient background. (*A*) Genotyping PCR showing efficient switching of *Mps1^{f}* to *Mps1^{DK}* in untransformed T cells. (*B*) Kaplan–Meier curves showing survival of *Mps1$^{f/+}$ p53$^{f/f}$* and *p53$^{f/f}$* mice in an Lck-Cre^{+} background. Note that the *p53$^{f/f}$* survival curve is the same curve presented in Fig. 2*D*. (*C*) Genomic PCRs showing full p53 deletion in the majority of the *Mps1$^{f/f}$ p53$^{f/f}$* and *p53$^{f/f}$* lymphomas and frequent *p53* loss of heterozygosity (LOH) in *Mps1$^{f/f}$ p53$^{f/+}$* lymphomas. Lane numbers are tumor identification numbers. (*D* and *E*) aCGH data showing loss of *p53* in tumors with the indicated genotypes. Each rectangle represents a single aCGH probe value. Three probe values are shown, for the deleted fragment (*Center*) and for the 5′ (*Left*) and 3′ (*Right*) regions flanking the deleted region. Log2 ratios in the range of −5 indicate complete loss of the probe and thus LOH of the wild-type *p53* allele in *Mps1$^{f/f}$ p53$^{f/+}$* tumors (*D*). The numbers on the left are tumor identification numbers (TID). (*F*) Kaplan–Meier survival curve showing survival of *Mps1$^{f/f}$*, *Mps1$^{f/f}$ p53$^{f/f}$*, *Mps1$^{f/f}$ p53$^{f/+}$*, and *p53$^{f/f}$* mice in a mouse mammary tumor virus (MMTV)-Cre^{+} background. (*G*) Genomic PCRs showing efficient excision of *Mps1* in the majority of *Mps1$^{f/f}$ p53$^{f/f}$* lymphomas. (*H*) Schematic overview of Mps1 RNA showing where the qPCR primers used in Fig. 2*G* and the RT-PCR primers used in Fig. S2*I* bind. (*I*) RT-PCR reactions on RNA isolated from *p53*-control tumors (TID 36 and 63), *Mps1$^{f/f}$ p53$^{f/+}$* (TID 13), and *Mps1$^{f/f}$ p53$^{f/f}$* (TID 23) tumors showing full penetrance of the truncated Mps1^{DK} allele in Mps1^{DK}-driven tumors. Primers 500 and 501 amplify murine Mps1 from the start codon to the stop codon; primers 500 and 503 amplify from the start codon to exon 5. Retroviral vectors encoding constructs for human GFP-Mps1^{DK} (pRetrox Mps1^{DK}) and GFP-Mps1^{WT} (pRetrox Mps1^{WT}) (used in Fig. 1*B*) serve as PCR controls. All RT-PCR products were Sanger sequenced, which confirmed deletion of the exons 3 and 4 in Mps1^{DK} tumors. (See Dataset S2 for information about the alignment the sequencing data.) (*J*) Quantification of interphase FISH measurements on untransformed *Mps1$^{f/f}$ Lck-Cre^{+}* T cells and *Mps1$^{f/f}$ p53$^{f/+}$ Lck-Cre^{+}* T-ALL cells.

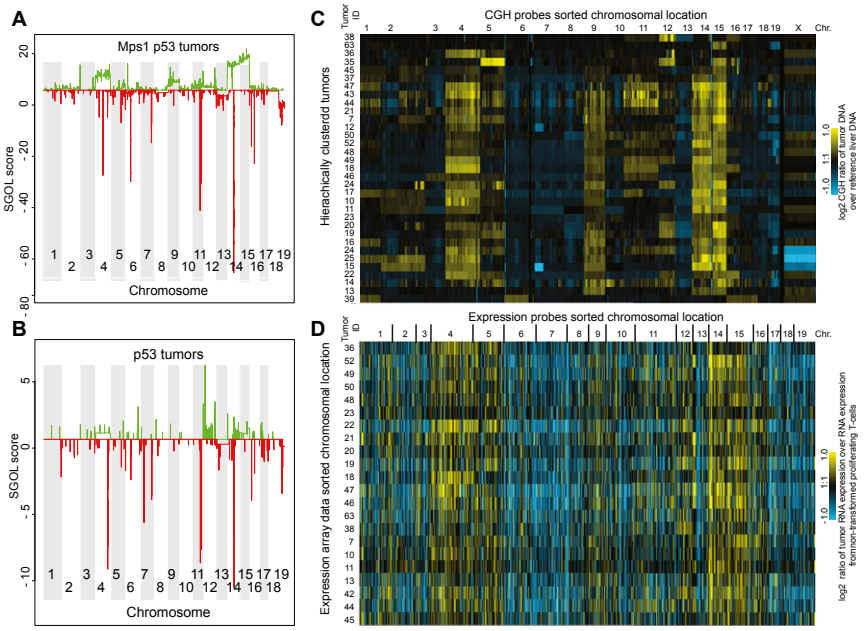

E

Pathway	Category	Observed	Expected	Enrichment	Raw p-value	Bonferroni-corrected p	Annotated in:
mRNA processing	411	90	53.02	1.7	2.30E-07	3.08E-05	Wiki pathways
T Cell Receptor Signaling Pathway	137	36	17.67	2.04	1.83E-05	0.0025	Wiki pathways
PluriNetWork	283	60	36.5	1.64	6.09E-05	0.0082	Wiki pathways
Translation Factors	44	16	5.68	2.82	6.56E-05	0.0088	Wiki pathways
Macrophage markers	9	6	1.16	5.17	0.0003	0.0402	Wiki pathways
Antigen processing and presentation	67	27	8.64	3.12	1.85E-08	3.64E-06	KEGG pathway
Primary immunodeficiency	33	16	4.26	3.76	7.43E-07	0.0001	KEGG pathway
Cell cycle	115	34	14.83	2.29	1.88E-06	0.0004	KEGG pathway
Allograft rejection	44	18	5.68	3.17	3.34E-06	0.0007	KEGG pathway
Intestinal immune network for IgA production	41	17	5.29	3.21	5.02E-06	0.001	KEGG pathway
Glioma	59	20	7.61	2.63	2.75E-05	0.0054	KEGG pathway
Phagosome	152	38	19.61	1.94	3.64E-05	0.0072	KEGG pathway
Graft-versus-host disease	43	16	5.55	2.88	4.74E-05	0.0093	KEGG pathway
Phosphatidylinositol signaling system	74	22	9.55	2.3	0.0001	0.0197	KEGG pathway
Systemic lupus erythematosus	70	21	9.03	2.33	0.0001	0.0197	KEGG pathway
Type I diabetes mellitus	51	17	6.58	2.58	0.0001	0.0197	KEGG pathway
Purine metabolism	154	37	19.86	1.86	0.0001	0.0197	KEGG pathway
Autoimmune thyroid disease	58	18	7.48	2.41	0.0002	0.0394	KEGG pathway
Metabolic process	8383	1355	1079.64	1.26	4.77E-35	2.22E-31	GO biological process
Gene expression	3644	665	469.31	1.42	9.19E-26	4.28E-22	GO biological process
Cellular biosynthetic process	3896	668	501.76	1.33	1.55E-18	7.22E-15	GO biological process
Biosynthetic process	4058	690	522.62	1.32	2.49E-18	1.16E-14	GO biological process
RNA metabolic process	2984	534	384.31	1.39	3.83E-18	1.78E-14	GO biological process
Regulation of cellular metabolic process	3683	622	474.33	1.31	1.41E-15	6.57E-12	GO biological process
T cell activation	295	89	37.99	2.34	3.06E-15	1.43E-11	GO biological process
Response to stress	1952	362	251.4	1.44	2.56E-14	1.19E-10	GO biological process
Regulation of gene expression	2845	494	366.4	1.35	3.30E-14	1.54E-10	GO biological process

Fig. S3. Common copy-number alterations and correlation between tumor copy-number changes and transcriptomes. (*A* and *B*) Cumulative SGOL scores for tumors arising in *Mps1 p53* (*A*) and *p53* (*B*) mice. (*C* and *D*) aCGH (*C*) and transcriptome data (*D*) sorted by chromosomal position. (*E*) Overview of pathways affected in aneuploid mouse tumors ($Mps1^{f/f}$ $p53^{f/f}$ and $Mps1^{f/f}$ $p53^{f/+}$) as analyzed using WebGestalt (1).

1. Zhang B, Kirov S, Snoddy J (2005) WebGestalt: An integrated system for exploring gene sets in various biological contexts. *Nucleic Acids Res* 33(Web Server issue):W741–748.

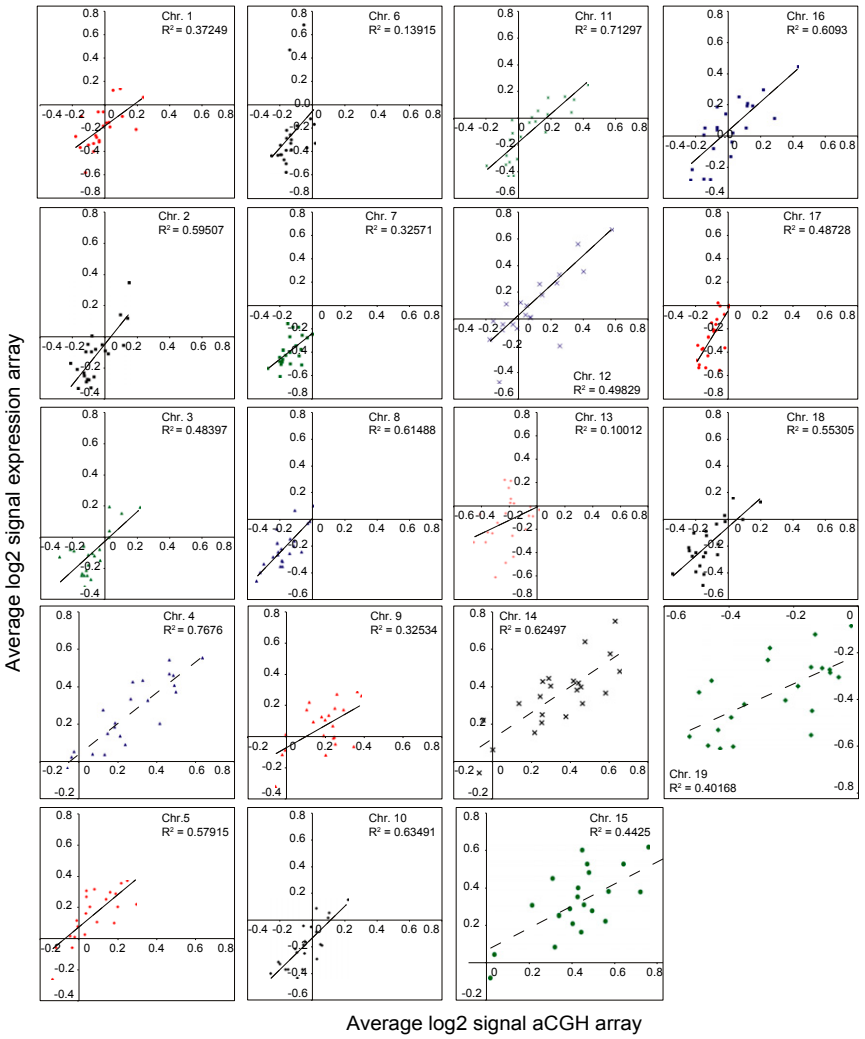

Fig. S4. Linear regression plots showing correlation strength (coefficient of correlation, R^2) between copy-number changes (aCGH) and expression changes (expression arrays) for all chromosomes and all tumors assessed by both aCGH and transcriptome analysis in this study.

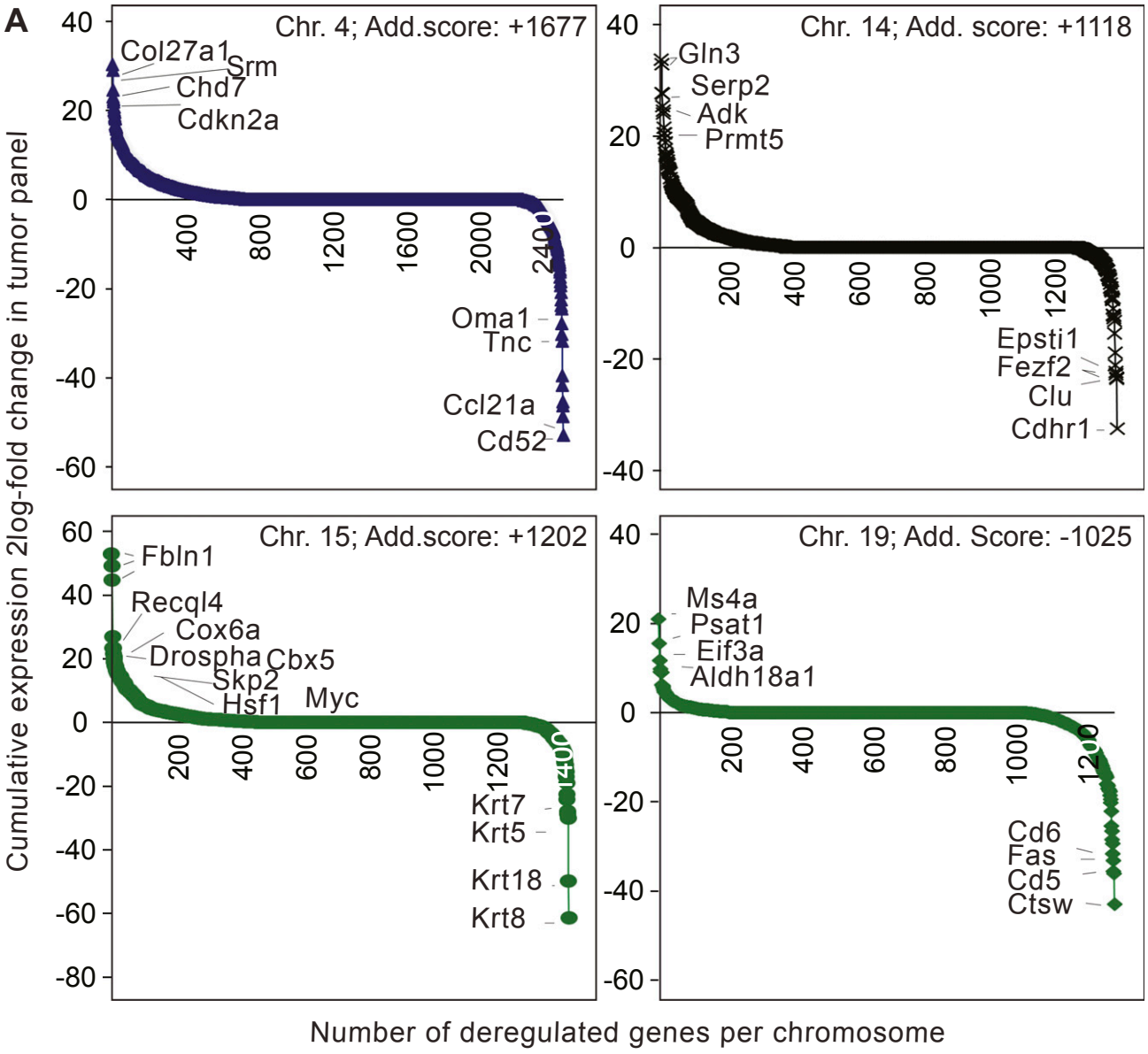

B

Genotype	%	Expected %
Mps1$^{+/+}$	38%	25%
Mps1$^{DK/+}$	62%	50%
Mps1$^{DK/DK}$	0%	25%

Live pups (n=237; 33 litters)

C

Genotype	%
Mps1$^{+/+}$	40%
Mps1$^{DK/+}$	41%
Reabsorbed embryos	19%

total number of embryos=96

Fig. S5. Mps1 truncation deregulates cellular metabolism and results in embryonic lethality. (*A*) Expression changes in individual genes sorted by cumulative expression score (the sum of expression changes within all tumors for that gene, additive or Add. score) sorted high to low for Chr4, Chr14, Chr15, and Chr19. (*B*) Total numbers of pups born from *Mps1*$^{DK/+}$ crosses. (*C*) Embryos ($n = 96$) harvested at E10.5 indicating embryonic lethality earlier than E10.5 for *Mps1*$^{DK/DK}$ mice. The high fraction of reabsorbed embryos also suggests lethality.

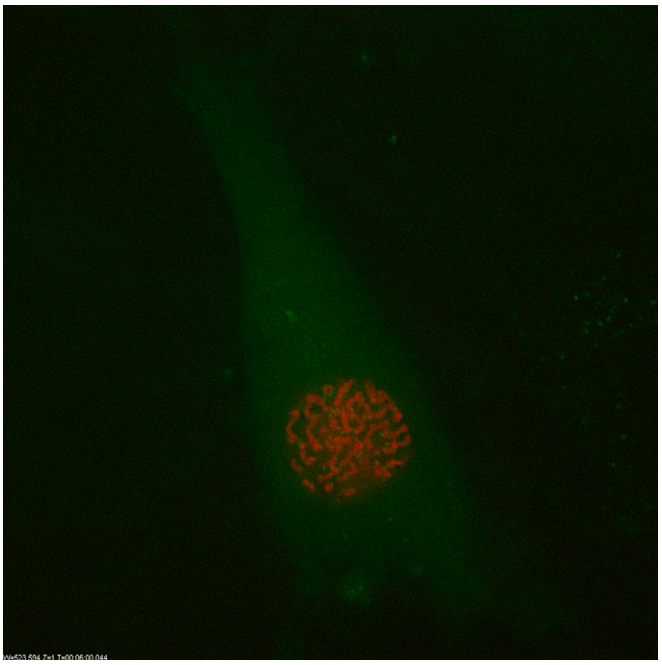

Movie S1. MEFs expressing GFP-tagged full-length Mps1 (green) coexpressing H2B-Cherry (red) showing kinetochore localization of full-length Mps1, but not Mps1^{DK}.

Movie S1

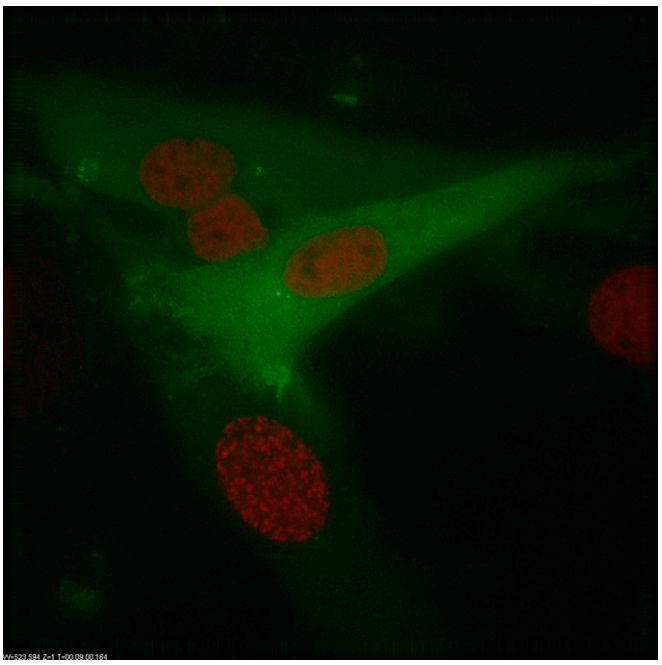

Movie S2. MEFs expressing GFP-tagged Mps1^{DK} (green) coexpressing H2B-Cherry (red) showing reduced kinetochore localization in Mps1^{DK}.

Movie S2

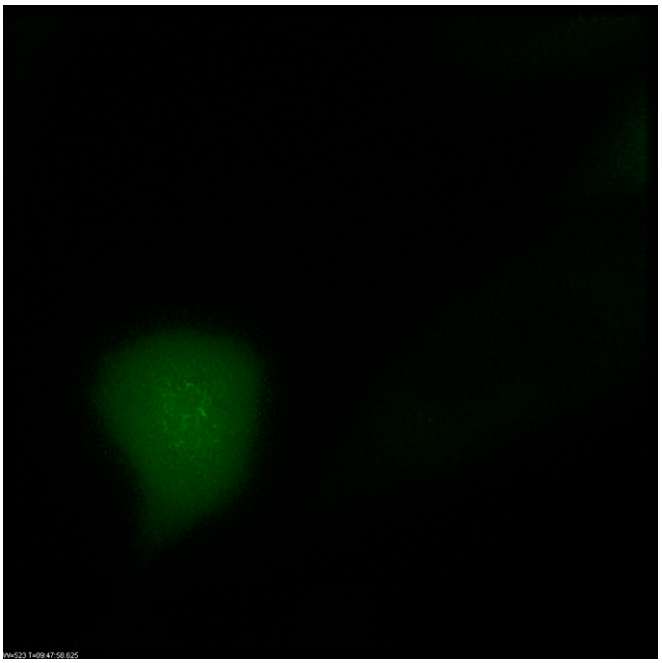

Movie S3. MCF 10A cells expressing GFP-tagged full-length Mps1 (green) showing strong kinetochore localization of full-length Mps1.

Movie S3

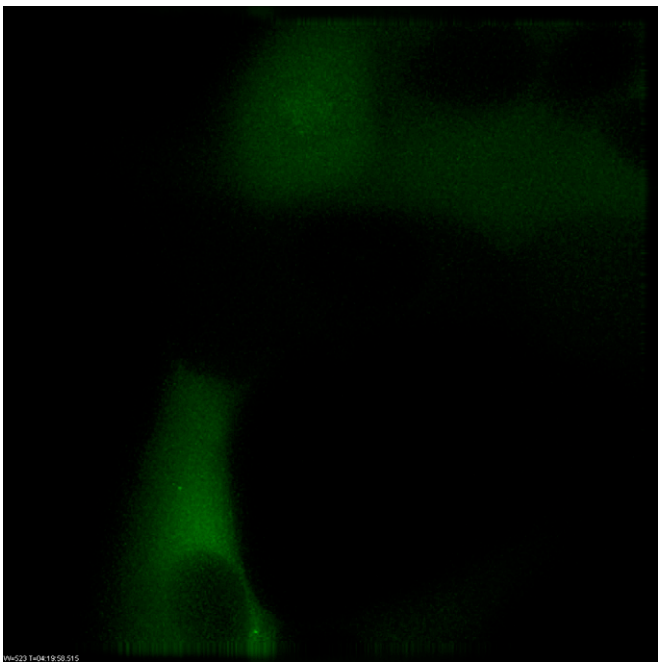

Movie S4. MCF 10A cells expressing GFP-tagged $Mps1^{DK}$ (green) showing weak kinetochore localization of $Mps1^{DK}$.

Movie S4

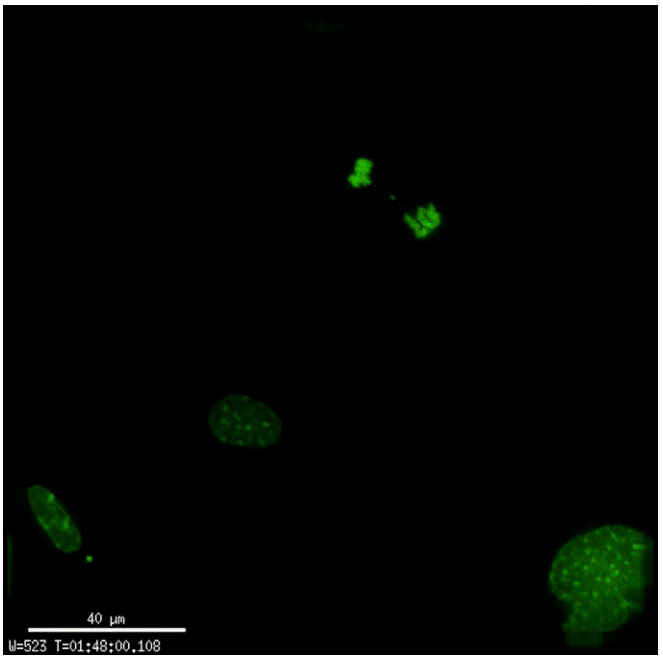

Movie S5. *Mps1*$^{f/f}$ MEFs expressing GFP-T2A-Cre showing lagging chromosomes coexpressing H2B-GFP.

Movie S5

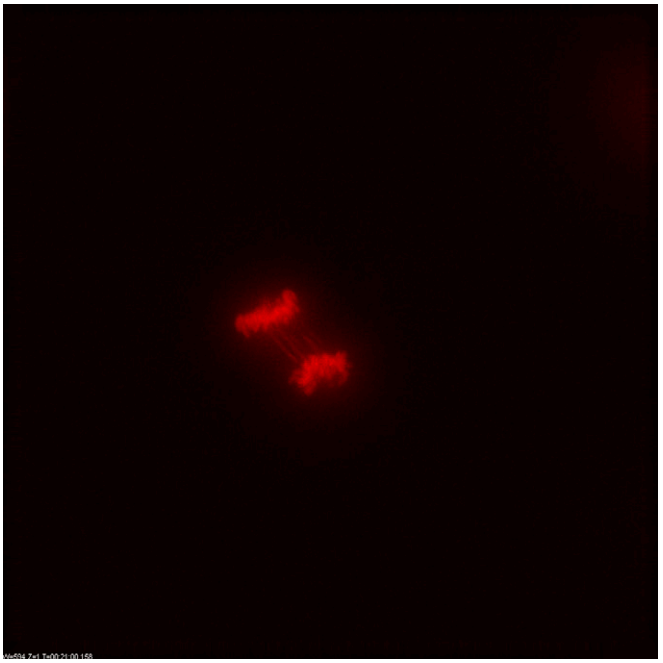

Movie S6. *Mps1*$^{f/f}$ MEFs expressing GFP-T2A-Cre showing lagging chromosomes coexpressing H2B-Cherry.

Movie S6

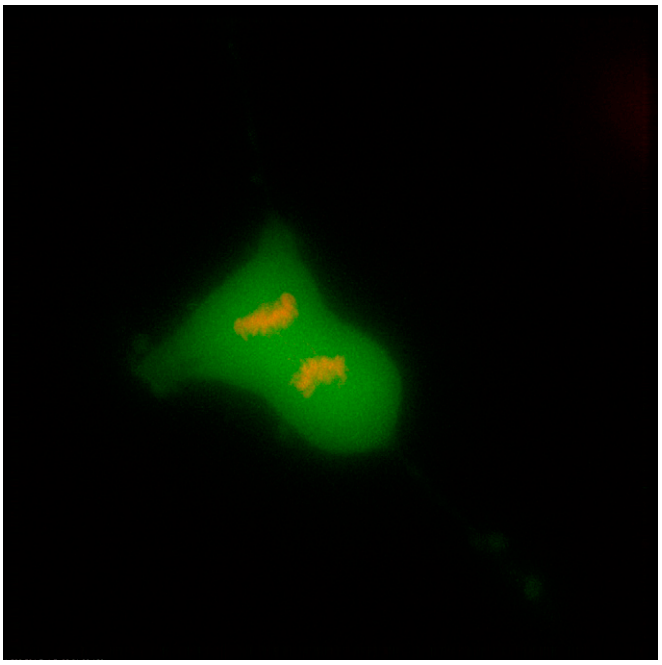

Movie S7. *Mps1*$^{f/f}$ MEFs expressing GFP-T2A-Cre showing lagging chromosomes coexpressing H2B-Cherry. Note: Movie S7 shows the same cell as Movie S6 but shows GFP-T2A-Cre expression to visualize cell morphology.

Movie S7

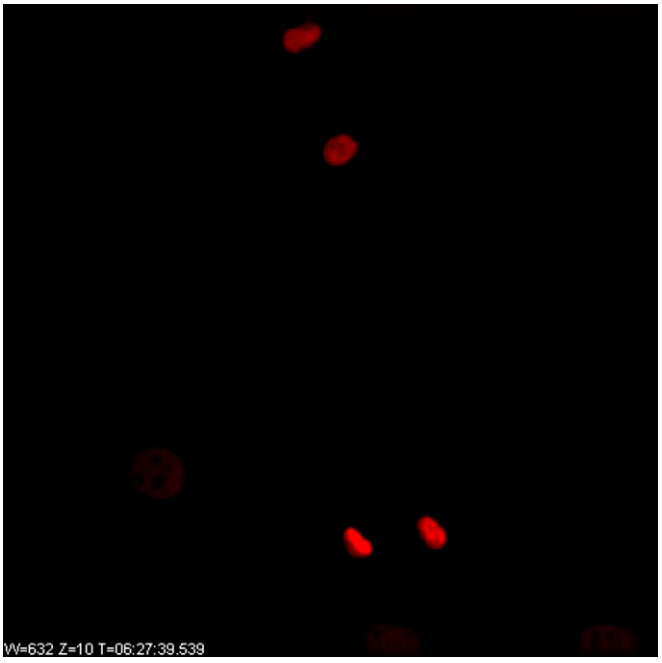

Movie S8. Control-infected *Mps1*$^{f/f}$ MEFs expressing H2B-Cherry showing unperturbed mitosis.

Movie S8

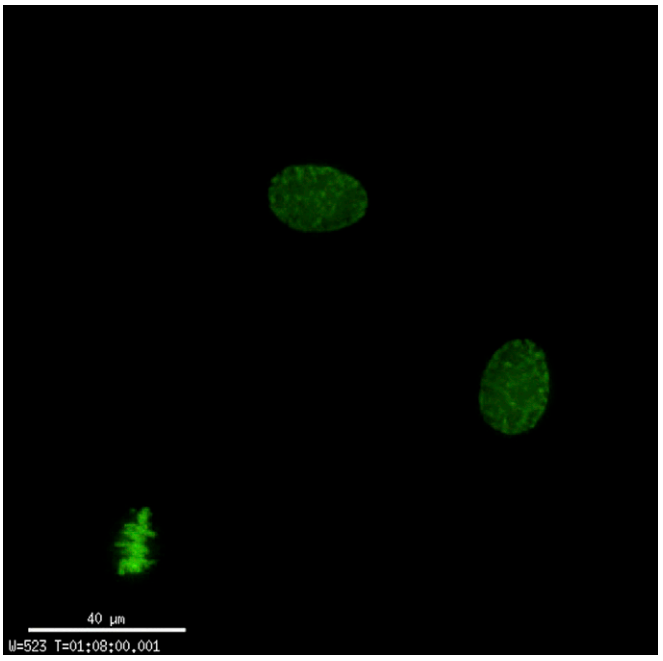

Movie S9. Control-infected *Mps1*$^{f/f}$ MEFs expressing H2B-GFP showing unperturbed mitosis.

Movie S9

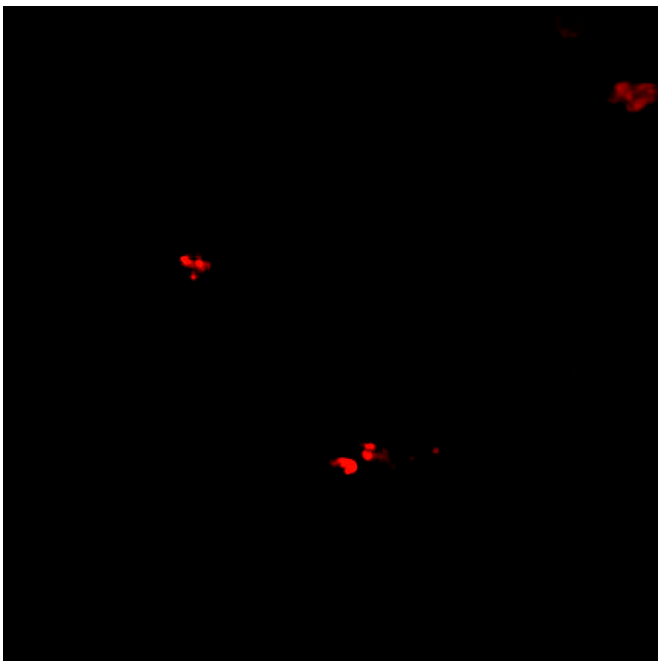

Movie S10. Cre–infected *Mps1*$^{f/f}$ MEFs expressing H2B-GFP showing failure to form a metaphase plate because of an alignment problem.

Movie S10

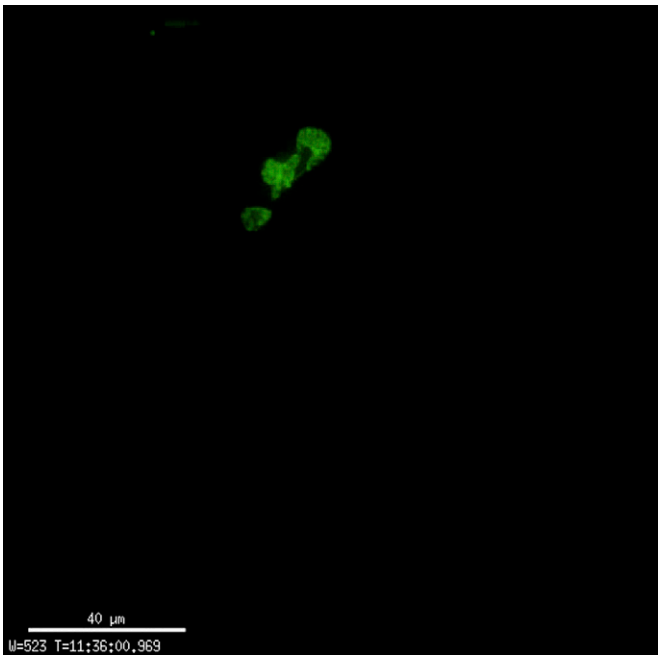

Movie S11. Cre-infected *Mps1*$^{f/f}$ MEFs expressing H2B-GFP showing failed chromosome alignment followed by tetraploidization.

Movie S11

Dataset S1. Genotyping and pathology information for all mice in this study including genotyping information of tumors

Dataset S1

Dataset S2. Alignments of Mps1 cDNA sequences generated from RNA isolated from tumors expressing full-length Mps1 or Mps1^{DK}, showing loss of the sequence encompassing exons 3 and 4 in Mps1^{DK} tumors

Dataset S2

Dataset S3. Normalized aCGH data for all assessed tumors and average aCGH data per chromosome

Dataset S3

Raw data have been deposited at in the National Center for Biotechnology Information Gene Expression Omnibus database under accession no. GSE57334.

Dataset S4. Normalized expression array data for all assessed tumors, average expression data per chromosome, and gene ontology analysis

Dataset S4

Raw data have been deposited at in the National Center for Biotechnology Information Gene Expression Omnibus database under accession no. GSE57334.

Dataset S5. Primer sequences used in this study

Dataset S5